

## Methyl orange adsorption by modified montmorillonite nanomaterials: Characterization, kinetic, isotherms and thermodynamic studies

Houria Rezala<sup>\*-1</sup>, Horiya Boukhatem<sup>1</sup>, Noreddine Boudechiche<sup>1,2</sup> & Amaya Romero<sup>3</sup>

<sup>1</sup>Faculty of Science and Technology, Djilali Bounaama University of Khemis-Miliana, Khemis-Miliana, Algeria.

<sup>2</sup>Laboratory of Reaction Engineering, Faculty of Mechanical Engineering and Process Engineering, USTHB, BP 32, 16111 Algiers, Algeria.

<sup>3</sup>Department of Chemical Engineering, Faculty of Chemistry, Castilla-La Mancha University, Ciudad Real, Spain.  
Email: rezala\_houria@hotmail.com

*Received 28 August 2022; accepted 29 September 2022*

Clays intercalated with cetyltrimethylammonium bromide (CTAB-Mt) and hydroxyl aluminium polycation have been prepared and analysed by X-ray fluorescence spectrometry, X-ray diffraction, fourier transform infrared spectroscopy, nitrogen adsorption-desorption at 77 K and thermal gravimetric analysis. The adsorption capacities of modified montmorillonite nanomaterials to remove methyl orange (MO) from aqueous solutions have been studied as a function of contact time, solution pH, adsorbent dosage and initial MO concentration at room temperature. The maximum removal efficiency of MO has been found in acidic medium, with 60 min equilibrium time and 1 g/L adsorbent dosage. The adsorption kinetics and isotherms have been well fitted by pseudo-second order and Langmuir models. The montmorillonites intercalated with both cetyltrimethylammonium bromide and hydroxyl aluminium polycation (CTAB-Al-Mt) have shown a high affinity for MO molecules. Thermodynamic results have indicated an exothermic, spontaneous and physical adsorption process. The characterization and adsorption performance of CTAB-Mt and CTAB-Al-Mt toward MO has also been compared with that of the hydroxyl-aluminium pillared montmorillonite (OH-Al-Mt) and purified montmorillonite (Na-Mt).

**Keywords:** Adsorption, Isotherm models, Kinetic models, Methyl orange, Montmorillonite nanomaterials

Methyl orange (MO) is an anionic dye which is extensively used in manufacturing printing paper, research laboratories, and textile industries. It can cause harmful effects such as diarrhoea, increased heart rate, cyanosis, vomiting, and tissue necrosis in human beings<sup>1,2</sup>. MO has light stability and low biodegradability thus difficult to remove from aqueous solutions by common water purification/treatment methods<sup>1</sup>. Hence, there is a continuing need to develop an effective method to treat MO effluents before releasing into the aquatic environment.

Several techniques have been used to remove MO from contaminated wastewater, including chemical oxidation<sup>3</sup>, electrocatalytic oxidation<sup>4</sup>, adsorption<sup>5-10</sup>, photocatalytic degradation<sup>11-13</sup>, and degradation by the combined electrochemical process<sup>14</sup>. Among these, adsorption has become the most desirable technique because of its benefits like low cost, ease of operation, simplicity of design, and insensitivity to toxic pollutants<sup>2</sup>. Activated carbon has been the most extensively used adsorbent due to its higher capacity for organic dyes adsorption. Nevertheless, because of the high cost of activated carbon, there is an

increasing interest in developing effective and cheaper adsorbents<sup>15</sup>.

Clay materials are being widely used in adsorption because of their low cost and abundance in nature. Montmorillonite is known as a good adsorbent because of its large specific surface area and high cation exchange capacity. However, anionic pollutants such as methyl orange adsorbs weakly on the montmorillonite because of the negative charges on its surface. Thus, the adsorption property of the montmorillonite can be improved through its modification using diverse techniques<sup>16</sup>. The modified montmorillonite by inorganic or organic compounds, such as polyoxo metal cations or surfactant cation, has a larger basal spacing and better porous structure. These properties are favourable for the adsorption of inorganic or organic pollutants, due mainly to the cation, ligand exchange or solution partition mechanism<sup>17</sup>.

The main objective of the present study was to investigate the adsorption of MO by CTAB-Mt or CTAB-Al-Mt. To the best of our knowledge, there is no report on the application of CTAB or both CTAB

and Al<sub>13</sub> modified nano-sized montmorillonite for removing MO from aqueous media. The resulting materials have been characterized by X-ray fluorescence spectrometry (XRF), X-ray diffraction (XRD), Fourier transform infrared spectroscopy (FTIR), nitrogen adsorption-desorption at 77 K and thermal gravimetric analysis (TGA). The effect of different parameters such as contact time, solution pH, adsorbent dose and initial dye concentration on the adsorption phenomena have been investigated by batch adsorption experiments. The kinetics and isotherm of adsorption process have been calculated. The adsorption performance of CTAB-Mt and CTAB-Al-Mt toward MO has also been compared with that of hydroxyl-aluminium pillared montmorillonite (OH-Al-Mt).

## Experimental Section

### Materials and chemicals

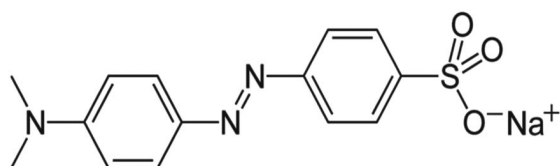
The raw bentonite used in this study was obtained from deposits of Maghnia in western Algeria. It was purified by a method reported elsewhere<sup>18</sup>. The obtained fraction with a particle size < 2 μm were referred to as Na-Mt and employed in the pillaring process.

The dye MO and all chemicals (C<sub>19</sub>H<sub>42</sub>BrN, Na<sub>2</sub>CO<sub>3</sub>, AlCl<sub>3</sub>.6H<sub>2</sub>O, NaOH, H<sub>2</sub>SO<sub>4</sub>) with the highest purity available were obtained from Biochem Chemopharma company, France and used as received. All the solutions were prepared using distilled water. Chemical structure of the MO is shown in Scheme 1.

### Adsorbents preparation

#### Preparation of cetyltrimethylammonium bromide intercalated montmorillonite

CTAB-Mt was prepared by following the procedure reported by Kiransan *et al.*<sup>19</sup>. An amount of CTAB equal to one of the cation exchange capacity of Na-Mt (CEC = 82.68 mmol/100g clay) was added with 1mass % of Na-Mt suspension under vigorous stirring at room temperature. After being stirred for 1 h, the mixture was centrifuged, followed by washing with distilled water and the solid was dried at 90°C for 24 h and grounded into powder.



Scheme 1— Molecular structure of MO.

#### Preparation of both cetyltrimethylammonium bromide and hydroxy aluminium polycation intercalated montmorillonite

Amounts of CTAB (0.3 g) and Al<sub>13</sub> (80 mL) were mixed to obtain CTAB-Al<sub>13</sub> mixed intercalation solution. The hydroxyl aluminium polycation Al<sub>13</sub> was prepared following the procedure reported by Rezala *et al.*<sup>20</sup> while the amounts of CTAB used above were equal to the one of the CEC of Na-Mt. The intercalation solution was added drop by drop to the water suspension of Na-Mt (1mass %) under stirring speed of 250 rpm at 80°C. The product was collected by centrifugation after stirring for 12 h at 80°C, and washed with distilled water, then dried at 80°C for 24 h and grounded into powder. This pillared sample was noted as CTAB-Al-Mt.

### Characterization methods

Chemical composition of the samples was determined by XRF using a model Philips Magix Pro spectrometer with X-ray tube and K $\alpha$  radiation for Rh. spectrometer contains two flows: Ar + Methane and scintillation flow. The XRD patterns were performed employing a Philips X'Pert MP diffractometer with Ni-filtered Cu K $\alpha$  radiation using a powder sample. FTIR of the samples were measured using a "Spectrum Two" (Perkin-Elmer, Inc.) spectrometer. The spectra range for KBr is 8300 – 350 cm<sup>-1</sup> for the optic system and between 6000 and 550 cm<sup>-1</sup> for ZnSe were performed with a resolution of 2 cm<sup>-1</sup>. TGA data were recorded on a Mettler Toledo TGA/DSC1 instrument; the samples were heated from room temperature to 1000°C (10°C/min) in air atmosphere. The derivative thermal gravimetric (DTG) curves were derived from the TG curves. Surface area and pore size distribution were determined by using N<sub>2</sub> as sorbate at 77 K in a static volumetric apparatus (Micrometrics ASAP 2010 sorptometer). Prior to each experiment, 0.2 g of sample was taken and subjected to a degassing process at 180°C for 16 h. Surface areas were calculated employing BET equation, while pore volumes were determined from N<sub>2</sub> uptake at a relative pressure (P/P<sub>0</sub>) of N<sub>2</sub> equal to 0.99. The characterization of OH-Al-Mt and Na-Mt was previously reported<sup>20</sup>.

### Adsorption experiments

Batch experiments were carried out in water bath shaker (HeidophUnimax 1010) using glass flasks by adding 1 g/L of adsorbent in 25 mL of initial 100 mg/L MO solutions and thermostated at 299 ± 1 K. The adsorption properties of these materials were studied as a function of contact time (5 - 240 min), solution pH (2 - 12), adsorbent dose (0.2 - 8g/L), initial MO concentration (4 - 200 mg/L) and

temperature (20, 30, 40 and 50°C) for optimizing operating conditions. Samples of 4 mL were withdrawn and centrifuged to separate the adsorbent from the solution. The supernatant was analyzed by UV–Vis spectrophotometer (selecta) at the maximum wavelength of absorption  $\lambda_{\max} = 466$  nm. The MO concentration of each experiment was carried out with calibration curves obtained by plotting the absorbance as a function of MO concentration.

The *pH* of MO solutions was adjusted using  $\text{H}_2\text{SO}_4$  (0.1 mol/L) and  $\text{NaOH}$  (0.1 mol/L) aqueous solutions, and was measured using a *pH* meter (Basic 20). The adsorption isotherm experiments were carried out by adding 1 g/L of adsorbents in 25 mL of MO solutions at different concentrations (4 – 200 mg/L) for desired contact time and *pH*. The amounts of adsorbed MO in the equilibrium per mass unit of the sample,  $q_e$  (mg/g), and the removal efficiency of the MO, *E* (%), were calculated according to Eqs (1) and (2), respectively:

$$q_e = (C_0 - C_e) * \frac{V}{m} \quad \dots(1)$$

$$E (\%) = \frac{C_0 - C_e}{C_0} * 100 \quad \dots(2)$$

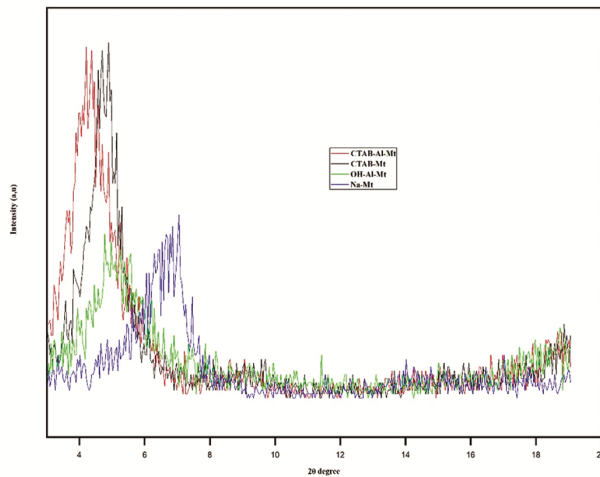


Fig. 1 — XRD patterns of Na-Mt, OH-Al-Mt, CTAB-Mt and CTAB-Al-Mt.

where,  $C_0$  is initial MO concentration (mg/L),  $C_e$  equilibrium MO concentration (mg/L),  $V$  the volume of MO solution (L), and  $m$  the mass of adsorbent(g).

## Results and Discussion

### Materials characterization

The XRF analysis has shown that the  $\text{Al}_2\text{O}_3$  content in CTAB-Al-Mt (18.39 mass %) is lower than that in OH-Al-Mt (25.26 mass %, see Ref 20). This fact is due to the existence of both CTAB and  $\text{Al}_{13}$  in the interlayer space, while the charge sites have occupied by the  $\text{Al}_{13}$  in OH-Al-Mt.

XRD patterns and relative basal spacing of the intercalated samples and the parent clay are illustrated in Fig. 1 and Table 1. The angle reflections due to the basal  $d_{001}$  reflection of silicate layers allowed obtaining information about the effect of intercalation on the basal spacing of the clay. In comparison with starting clay, the  $d_{001}$  peak of intercalated samples is shifted to lower angle, indicating the enlargement of basal spacing of clay as a consequence of intercalation of organic and/or inorganic species into montmorillonite (from 1.25 nm in parent clay to about 1.85 nm in OH-Al-Mt, 1.81 nm in CTAB-Mt and 2.14 nm in CTAB-Al-Mt). These observations are in agreement with results previously reported<sup>16,21,22</sup>. Figure 1 also shows that the peak corresponding to the diffraction of the (001) plane is larger in the case of CTAB-Al-Mt. This is in line with previous results indicating that CTAB and  $\text{Al}_{13}$  simultaneously exist in the interlayer spaces<sup>23</sup>.

The textural properties of the samples are shown in Table 1. It is evident that the BET surface area and pore volume of CTAB-Mt and CTAB-Al-Mt have significantly lower than that of Na-Mt due to the fact that the CTAB molecules penetrated into the montmorillonite interlayer spaces and blocked the access to  $\text{N}_2$  molecules. Moreover, OH-Al-Mt has the highest BET surface area and pore volume which is attributed to the expansion of the montmorillonite interlayer space by  $\text{Al}_{13}$  and creation of interlamellar pores with low average pore diameter<sup>24</sup>.

Table 1 — Basal spacing ( $d_{001}$ ) and textural properties of Na-Mt, OH-Al-Mt, CTAB-Mt and CTAB-Al-Mt (data of Na-Mt and OH-Al-Mt were taken from Ref 20).

| Adsorbent  | Basal spacing $d_{001}$ (nm) | BET Surface area ( $\text{m}^2/\text{g}$ ) | Pore volume ( $\text{cm}^3/\text{g}$ ) | Average pore diameter (nm) |
|------------|------------------------------|--|--|----------------------------|
| Na-Mt      | 1.25                         | 59.3                                       | 0.115                                  | 7.75                       |
| OH-Al-Mt   | 1.85                         | 182.9                                      | 0.179                                  | 3.92                       |
| CTAB-Mt    | 1.81                         | 10.0                                       | 0.057                                  | 24.77                      |
| CTAB-Al-Mt | 2.14                         | 15.3                                       | 0.112                                  | 29.30                      |

Figure 2 reports the  $N_2$  adsorption–desorption isotherms of CTAB-Mt and CTAB-Al-Mt. The Na-Mt and OH-Al-Mt curves have also presented for comparison. All the samples exhibited Type II isotherms according to the International Union of Pure and Applied Chemistry (IUPAC) classification<sup>25</sup>, which is the normal form of isotherm has obtained with macroporous or non-porous adsorbents. Also, an H3-type hysteresis, characteristic of agglomerates of slit-shaped pores with non-uniform sizes and shapes could be observed. It is understandable that the samples have porous media containing both macropores and mesopores. Nitrogen molecules first diffuse into the micropore under extremely low pressure. Further nitrogen molecules are adsorbed in a monolayer state and in subsequent layers on condensation when relative pressure continually increases.

The FTIR spectra of parent montmorillonite and modified montmorillonite samples in the range of  $4000\text{--}400\text{ cm}^{-1}$  are shown in Fig. 3. The spectra of CTAB-Mt and CTAB-Al-Mt have shown three new absorption bands at  $2934$ ,  $2851$  and  $1482\text{ cm}^{-1}$ , which are attributed to the asymmetric stretching vibrations of C–H groups, symmetric stretching vibrations of C–H groups and C–H symmetric bending of (N+)–CH<sub>3</sub> groups from cetyltrimethylammonium (CTAB), respectively<sup>19,26</sup>. The absence of these bands in the spectra of Na-Mt and OH-Al-Mt, confirms the existence of CTAB in the montmorillonite structure. The intensities of these bands increased with increasing CTAB loading amounts. The absorption bands at  $3617$  and  $1634\text{ cm}^{-1}$  of the modified montmorillonite samples, corresponding to the stretching vibration of

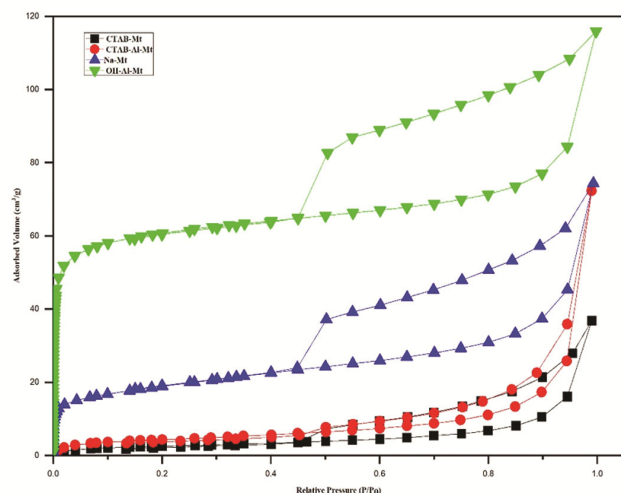


Fig. 2 — Nitrogen adsorption-desorption isotherms of Na-Mt, OH-Al-Mt, CTAB-Mt and CTAB-Al-Mt.

octahedral OH groups and OH deformation of interlayer water have diminished in intensity compared with those of Na-Mt, which may be due to the structural changes from hydrophilic to hydrophobic character<sup>22,27</sup>. The bands at  $515$ ,  $463$  and  $1000\text{ cm}^{-1}$  characterize the montmorillonite and correspond to the Si–O bending and stretching vibrations while the band at  $622\text{ cm}^{-1}$  is attributable to aluminium–oxygen bonds of the lattice<sup>28</sup>.

Thermal gravimetric and derivative thermal gravimetric curves of CTAB-Mt and CTAB-Al-Mt are depicted in Fig. 4. The TG curves exhibit continuous mass loss. The first mass loss has observed at  $25\text{--}200^\circ\text{C}$  temperature range with DTG peaks centered at  $26$  and  $58^\circ\text{C}$  for CTAB-Mt and CTAB-Al-Mt, respectively, corresponding to the physically adsorbed water on the external surface

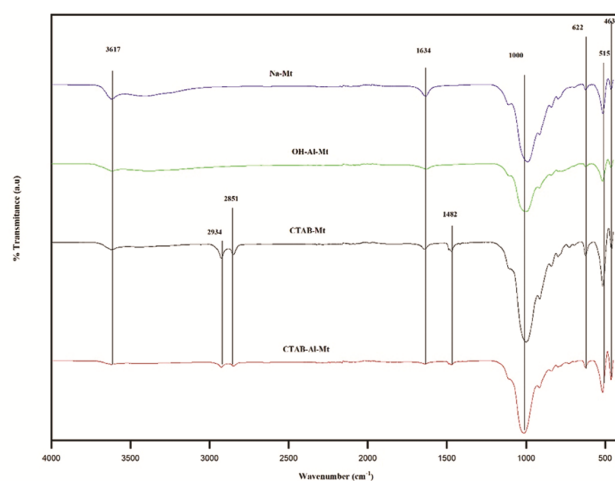


Fig. 3 — FTIR spectra of Na-Mt, OH-Al-Mt, CTAB-Mt and CTAB-Al-Mt.

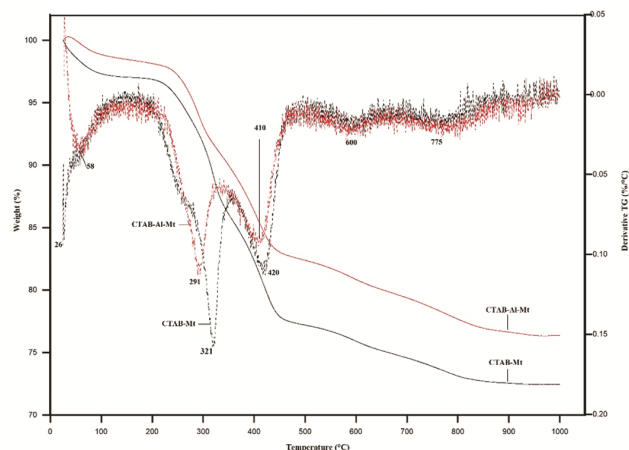


Fig. 4 — TGA (Solid line) and DTG (dashed line) curves for CTAB-Mt and CTAB-Al-Mt.

and inside the interlayer space of intercalated montmorillonite<sup>29,30</sup>. The significant mass loss in the temperature range of 200-500 °C with DTG peaks centered at 321, 420 °C for CTAB-Mt and 291, 410 °C for CTAB-Al-Mt, have related to the decomposition of loaded surfactant. An additional contribution should originate from dehydroxylation of interlayer Al<sub>13</sub> cations present in the CTAB-Al-Mt<sup>27,30-32</sup>. The last small mass loss from 500-1000 °C associated with the DTG small peaks at 600 and 775 °C, have attributed to the dehydroxylation of hydroxyl groups in the aluminosilicate structure<sup>29-31,33,34</sup>. Moreover, the CTAB-Al-Mt in the temperature range has lower mass loss compared to CTAB-Mt, indicating that this material presented low thermal stability and low content of surfactant molecules<sup>33,35</sup>. According to the literature studies<sup>36,37</sup>, the loaded surfactant in the modified montmorillonite samples can be calculated using the following equation (3):

$$X = S * 10^5 / \text{CEC} * (M - Y) * (100 - S) \dots (3)$$

where, X is the loaded surfactant amount (loaded CTAB); S is the mass loss percentage of surfactant in the sample; M is the molecular mass of surfactant ( $M_{W_{\text{CTAB}}} = 364.45$ ); Y is 0 when the surfactant is molecule (i.e., CTAB) and 80 (the molecular mass of Br) when the surfactant is cation (i.e., CTA+)

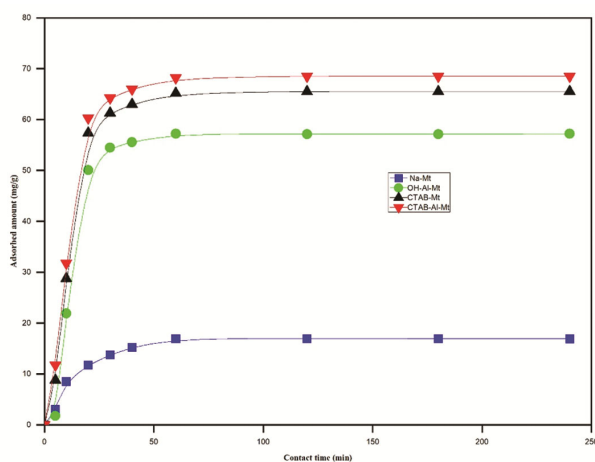


Fig. 5 — Effect of contact time on MO removal (MO: 100 mg/L, adsorbent dose: 1 g/L).

The loaded amount of CTAB molecules adsorbed in the interlayer spaces of montmorillonite have determined from the mass %loss of TG curves occurred between 200 and 500 °C found to be 0.81 CEC and 0.62 CEC for CTAB-Mt and CTAB-Al-Mt, respectively.

#### MO adsorption on montmorillonite samples

The influence of contact time on the adsorption capacities of different materials for MO is depicted in Fig. 5. All the samples have shown fast adsorption at initial 10 min and a slower adsorption followed by an equilibrium adsorption within 60 min. The maximum adsorption of MO onto different materials is observed at 60 min which is chosen as the optimum contact time.

In order to investigate the adsorption kinetics and mechanism of MO adsorption on different materials, pseudo-first order and pseudo-second order models have been used to fit the kinetics process. The pseudo-first-order equation in linear form<sup>38</sup> is given by:

$$\log(q_e - q_t) = \log q_e - \left( \frac{k_1}{2.303} \right) t \quad \dots (4)$$

and the expression of linear form of pseudo-second-order model<sup>39,40</sup> is given as:

$$t/q_t = \left( \frac{1}{k_2 q_e^2} \right) + (1/q_e) t \quad \dots (5)$$

Where,  $q_e$  and  $q_t$  are the amounts of MO ( $\text{mg g}^{-1}$ ) adsorbed on the adsorbent at equilibrium and at a given time  $t$  (min), respectively.  $k_1$  ( $\text{min}^{-1}$ ) and  $k_2$  ( $\text{g/mg.min}$ ) are the pseudo-first-order and pseudo-second-order rate constants, respectively.

Table 2 illustrates the kinetic parameters and correlation coefficient values. It is found that, of the different adsorbents, the pseudo-second-order model fitted well with the experimental results with  $R^2 = 0.99$ . Similar reports are available in literature<sup>23,41-43</sup>.

The effects of solution pH on adsorbents have been examined and the results are presented in Fig. 6. The data indicate the removal of MO decreased with increasing pH solution from 2 to 12. It is clear that the

Table 2 — Adsorption kinetics parameters of MO on Na-Mt, OH-Al-Mt, CTAB-Mt and CTAB-Al-Mt.

| Adsorbent  | Pseudo-first order model |                             |        | Pseudo-second order model |                       |       |
|------------|--------------------------|-----------------------------|--------|---------------------------|-----------------------|-------|
|            | $q_e$ (mg/g)             | $k_1$ ( $\text{min}^{-1}$ ) | $R^2$  | $q_e$ (mg/g)              | $k_2$ (g/mg. min)     | $R^2$ |
| Na-Mt      | 16.59                    | 0.0515                      | 0.989  | 17.60                     | $7.6 \times 10^{-3}$  | 0.994 |
| OH-Al-Mt   | 84.33                    | 0.1059                      | 0.965  | 62.5                      | $2.6 \times 10^{-3}$  | 0.996 |
| CTAB-Mt    | 80.37                    | 0.096                       | 0.9631 | 69.93                     | $1.2 \times 10^{-3}$  | 0.986 |
| CTAB-Al-Mt | 78.52                    | 0.092                       | 0.958  | 71.42                     | $3.02 \times 10^{-3}$ | 0.998 |

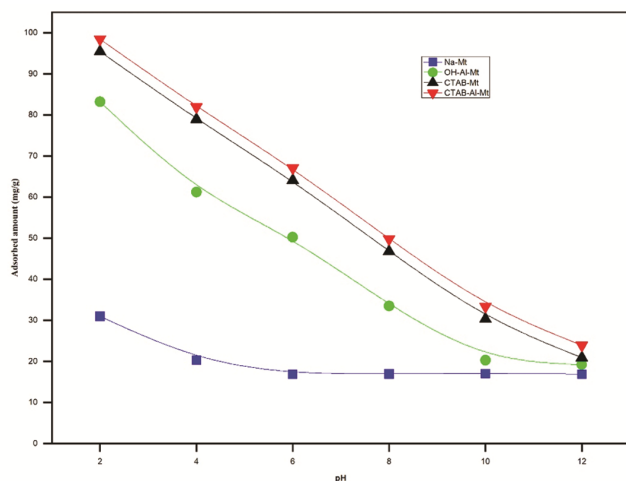


Fig. 6 — Effect of solution pH on the adsorption of MO (MO: 100 mg/L, adsorbent dose: 1 g/L, contact time: 60 min).

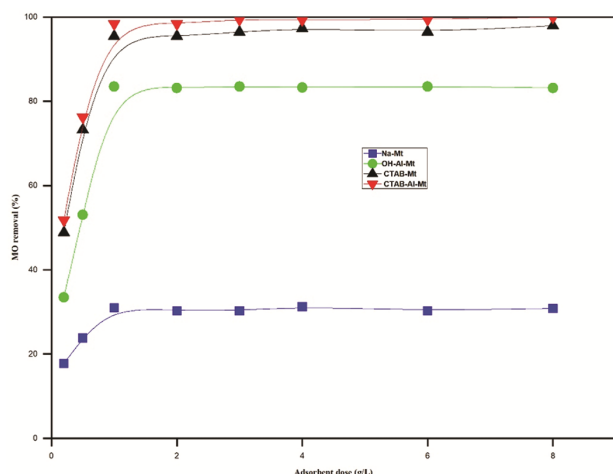


Fig. 7 — Effect of adsorbent dose on MO removal (MO: 100 mg/L, contact time: 60 min, pH: 2).

adsorption capacity of MO is maximum at pH 2. This fact may be attributed to the high electrostatic attractions between the negative charges of MO and the positive charges of different adsorbents in aqueous acidic solutions. In contrast, in alkaline regions, the negatively charged surface of adsorbents does not favour the uptake of anionic dye MO due to the electrostatic repulsion. Additionally, increasing pH values led to increasing the amount of OH<sup>-</sup> ions competing with dye anions for the adsorption onto materials. Similar results have been reported by previous works<sup>19,27</sup>. According to these results, the optimum pH of 2 is fixed in the successive experiments.

The effect of adsorbent dosage on MO adsorption is shown in Fig. 7. As can be seen, the % removal MO

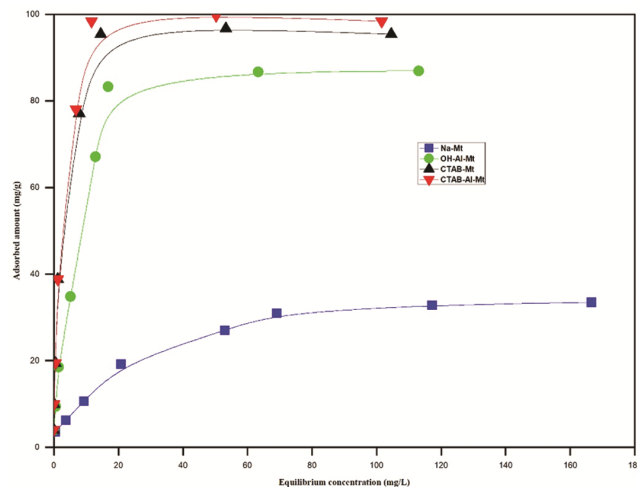


Fig. 8 — Adsorption isotherms of MO onto Na-Mt, OH-Al-Mt, CTAB-Mt and CTAB-Al-Mt (contact time: 60 min, adsorbent dose: 1 g/L, pH: 2).

increased as adsorbent concentration increased until the mass concentration reaches 1 g/L. This behaviour is due to the increased availability of adsorption sites as the adsorbent concentration increases, until equilibrium adsorption is reached, indicating saturation of the adsorption sites. Considering the cost of adsorbents and effectiveness of elimination, the optimum adsorbent dosage is fixed at 1 g/L for the further experiments.

The adsorption isotherms have carried out at different initial concentrations (4 to 200 mg/L) during 60 min at room temperature, pH of 2 and adsorbent dose 1g/L. The isotherms are formed by plot adsorbed amount of MO versus equilibrium concentration. Figure 8 depicts the adsorption of MO by all the materials. It can be seen that for all the adsorbents, the amount of MO adsorbed increases with an increase in initial MO concentration, due to the increased driving force of the concentration gradient<sup>44,45</sup>. Further the rate of adsorption is reduced until reaching equilibrium, which corresponds to 33 mg/g, 86 mg/g, 96 mg/g and 99 mg/g for Na-Mt, OH-Al-Mt, CTAB-Mt and CTAB-Al-Mt, respectively.

In order to comprehend the interactions between MO and the adsorbents, adsorption isotherm models Langmuir<sup>46</sup>, Freundlich<sup>47</sup> and Temkin<sup>48</sup> have been tested. The linear forms of Langmuir, Freundlich and Temkin models are expressed using Eqs (6), (7) and (8), respectively:

$$C_e/q_e = \frac{1}{K_L \cdot q_m} + (1/q_m) C_e \quad \dots(6)$$

$$\log q_e = \log K_F + (1/n) \log C_e \quad \dots(7)$$

Table 3 — Isotherm model parameters for adsorption of MO onto Na-Mt, OH-Al-Mt, CTAB-Mt and CTAB-Al-Mt.

| Adsorbent  | Langmuir        |                 |       |       | Freundlich      |       | Temkin |                 |       |
|------------|-----------------|-----------------|-------|-------|-----------------|-------|--------|-----------------|-------|
|            | $q_m$<br>(mg/g) | $K_L$<br>(L/mg) | $R^2$ | $1/n$ | $K_F$<br>(mg/g) | $R^2$ | $B_T$  | $K_T$<br>(L/mg) | $R^2$ |
| Na-Mt      | 36.76           | 0.0632          | 0.99  | 0.416 | 4.61            | 0.96  | 0.155  | 0.244           | 0.90  |
| OH-Al-Mt   | 91.74           | 0.20            | 0.99  | 0.46  | 14.78           | 0.93  | 14.64  | 5.11            | 0.90  |
| CTAB-Mt    | 100             | 0.909           | 0.999 | 0.336 | 29.785          | 0.90  | 12.20  | 42.55           | 0.91  |
| CTAB-Al-Mt | 111             | 0.83            | 0.999 | 0.375 | 27.22           | 0.937 | 12.69  | 41.76           | 0.906 |

$$q_e = B_T \ln K_T + B_T \ln C_e \quad \dots(8)$$

Where,  $q_m$  (mg/g) and  $K_L$  (L/mg) are Langmuir constants respectively related to maximum adsorption capacity and adsorption energy.  $K_F$  and  $n$  are Freundlich constants respectively related to adsorption capacity ((mg/g)(L/mg)<sup>n</sup>) and adsorption intensity.  $B_T = RT/b$ ,  $T$  is the absolute temperature (K),  $R$  is the universal gas constant (8.314 J/mol.K), and  $b$  is the Temkin constant related to heat of adsorption (J/mol).

The fitted constants for Langmuir, Freundlich and Temkin isotherm models at room temperature are summarized in Table 3. The coefficient of determination ( $R^2$ ) values in the Langmuir isotherm model are above 0.99, which is higher than the  $R^2$  for Freundlich and Temkin isotherms, indicating best fit by this model. Langmuir model explains monolayer adsorption process which product on homogeny surface of adsorbent. The essential characteristics of the Langmuir equation can be expressed in terms of a dimensionless separation factor,  $R_L$ , defined as <sup>49</sup>:

$$R_L = \frac{1}{1 + K_L C_0} \quad \dots (9)$$

Generally, adsorption of any contaminant is considered favourable ( $0 < R_L < 1$ ); unfavourable ( $R_L > 1$ ), linear ( $R_L = 1$ ) and irreversible ( $R_L = 0$ )<sup>49</sup>. The measured  $R_L$  are below to the unit ( $0.005 < R_L < 0.8$ ), indicated the favourable adsorption of MO onto adsorbents.

Based on the above results (Fig. 5 to Fig. 8), it can be seen that the MO adsorption by the different adsorbents decreases in the following order: CTAB-Al-Mt > CTAB-Mt > OH-Al-Mt > Na-Mt. CTAB-Al-Mt has the best adsorption capacity toward MO and can be due to: (i) large basal spacing (21.4 Å), (ii) anion-exchange process between the anion of CTAB (Br-) and anion of MO ( $C_{14}H_{14}N_3SO_3^-$ ) and (iii) anion/ligand exchange as CTAB-Al-Mt is multifunctional adsorbent. However, CTAB-Mt is in the second order and can be attributed to: (i) anion exchange process already explained and (ii)

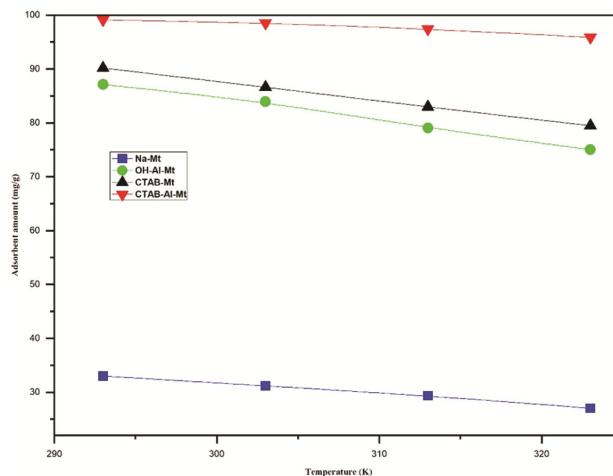


Fig. 9 — Effects of temperature on the MO adsorption capacity of Na-Mt, OH-Al-Mt, CTAB-Mt and CTAB-Al-Mt (MO: 100 mg/L, contact time: 60 min, adsorbent dose: 1 g/L, pH: 2).

hydrophobic interactions between MO and CTAB. In contrast, OH-Al-Mt and Na-Mt has the lowest adsorption capacities and can uptake MO by: (i) electrostatic attraction between the negative charges of the MO and the positive charges of both adsorbents and (ii) ion exchange between MO and surface  $\text{OH}$  groups or hydroxide groups of  $\text{Al}_{13}$  penetrated into the montmorillonite interlayer spaces. Similar results have been obtained by previously reports<sup>17,23</sup>.

Recently, there are a few articles that worked on the MO adsorption by clays and cited their highest removal efficiency ( $E\%$ ). Our adsorbent CTAB-Al-Mt shows a high affinity for MO molecules and the removal efficiency (99%) which is much higher to that in previous results (96.4% for organic matter-rich clays from Egypt<sup>50</sup>, 92.9 % for calcinated organic matter-rich clays from Egypt<sup>51</sup> and 98% for cetyltrimethylammoniumbromide/ $\text{H}_2\text{O}_2$ -clay<sup>51</sup>).

Temperature is an important parameter for the adsorption process. A plot of the MO uptake as a function of temperature (293, 303, 313 and 323 K) and is shown in Fig. 9. The adsorbed amounts of MO are decreased as temperature increased. The result revealed that adsorption onto the adsorbents is favorable at low

Table 4 — Thermodynamics parameters of MO adsorption onto the Na-Mt, OH-Al-Mt, CTAB-Mt and CTAB-Al-Mt.

| Adsorbent  | $\Delta H^\circ$ (kJ/mol) | $\Delta S^\circ$ (J/mol.K) | $\Delta G^\circ$ (kJ/mol) |         |        |        |
|------------|---------------------------|----------------------------|---------------------------|---------|--------|--------|
|            |                           |                            | 293 K                     | 303 K   | 313 K  | 323 K  |
| Na-Mt      | -5.929                    | -26.131                    | 1.727                     | 1.988   | 2.250  | 2.511  |
| OH-Al-Mt   | -16.900                   | -42.048                    | -4.580                    | -4.160  | -3.739 | -3.319 |
| CTAB-Mt    | -17.472                   | -41.758                    | -5.237                    | -4.819  | -4.402 | -3.984 |
| CTAB-Al-Mt | -32.125                   | -71.038                    | -11.100                   | -10.382 | -9.664 | -8.947 |

temperature and thus suggesting that the adsorption process is exothermic (as the adsorbate is adsorbed on the surface, the adsorbent energy decreases, resulting in heat evolution). Temperature is a crucial parameter in physical adsorption reactions. Thus, adsorption decreases with increase in temperature and molecules adsorbed earlier on a surface tend to desorb from the surface at elevated temperatures<sup>45</sup>. This may be due to the tendency of dye molecules to escape from the solid phase to the bulk phase with an increase in temperature of the solution<sup>52</sup>.

Thermodynamic parameters which include the change in Gibbs's free energy ( $\Delta G^\circ$ : kJ/mol), enthalpy ( $\Delta H^\circ$ : kJ/mol) and entropy ( $\Delta S^\circ$ : J/mol.K) were used to define the thermodynamic behavior of the adsorption of MO onto the adsorbents and were calculated using the following equations<sup>52</sup>:

$$\ln(q_e m / C_e) = (\Delta S^\circ / R) - (\Delta H^\circ / RT) \quad \dots (10)$$

$$\Delta G^\circ = \Delta H^\circ - T * \Delta S^\circ \quad \dots (11)$$

where,  $m$  is the adsorbent dose (g/L),  $C_e$  the equilibrium concentration (mg/L) of the MO in solution,  $R$  is the gas constant (8.314 J/mol.K) and  $T$  is the absolute temperature (K).

The values of  $\Delta H^\circ$  and  $\Delta S^\circ$  have calculated from the slope ( $-\Delta H^\circ / R$ ) and intercept ( $\Delta S^\circ / R$ ) of plots of  $\ln(q_e / C_e)$  against  $1/T$  (figure not shown). The  $\Delta G^\circ$  values have calculated using Eq. (11). The determined values of the thermodynamic parameters are summarized in Table 4. The values of  $\Delta G^\circ$  are negative for OH-Al-Mt, CTAB-Mt and CTAB-Al-Mt and positive for Na-Mt, indicating that the adsorption of MO on OH-Al-Mt, CTAB-Mt and CTAB-Al-Mt was spontaneous process under the experimental conditions, while it is a non-spontaneous process for Na-Mt.

The negative value of  $\Delta H^\circ$  suggests that the adsorption of MO onto adsorbents is exothermic and the negative  $\Delta S^\circ$  value suggested a decline in the disorder at the solid/solution interface during the adsorption.

Generally, the adsorption is physical when the  $\Delta H^\circ$  is less than 25 kJ/mol and is chemical when  $\Delta H^\circ$  is in the range of 40–200 kJ/mol<sup>53</sup>. In this work,  $\Delta H^\circ$  is

less than 25 kJ/mol and thus physical adsorption is predominant.

#### Possible strategies for regeneration

Regeneration is defined as the rapid recycling or recovery of spent adsorbents using technically and economically feasible methods. A number of regeneration methods, including thermal regeneration, steam regeneration, pressure swing regeneration, vacuum regeneration, microwave regeneration, ultrasound regeneration, chemical regeneration, oxidative regeneration, ozone regeneration, bio-regeneration and electrochemical regeneration have been employed to retain the adsorption capacity of adsorbents. In our research, adsorption is physical, the possible strategies for regeneration of the modified clays after MO adsorption are chemical regeneration method with propanone, ethanol or ethanoic acid as eluents. The use of these solvents is due to their properties of dissolving other substances without destroying their structure.

#### Conclusion

CTAB-Mt, OH-Al-Mt and CTAB-Al-Mt have been prepared and characterized by XRF, XRD, FTIR, BET analysis and TGA. The characterization results confirm the intercalation of organic and/or inorganic species into montmorillonite. The optimized conditions for MO dye removal by different adsorbents have been confirmed at 1 g/L adsorbent dosage, equilibrium time 60 min and acid pH (2). The MO adsorption by the different adsorbents decreased in the following order: CTAB-Al-Mt > CTAB-Mt > OH-Al-Mt > Na-Mt. The adsorption kinetic of MO onto the modified montmorillonite samples can be well fitted by the pseudo second-order model and the adsorption isotherm is in good fit by the Langmuir model. Thermodynamic studies have shown that the adsorption is spontaneous, exothermic and is a physical process.

#### Acknowledgements

This work was supported by Process Engineering and Analysis Laboratories, Djilali BOUNAAMA of

Khemis-Miliana University (Algeria) and Catalysis Laboratory, Castilla-La Mancha University (Spain).

## References

- 1 Sejie F P & Nadiye-Tabbiruka M S, *Phys Chem*, 6 (2016) 39.
- 2 Klett C, Barry A, Balti I, Lelli P, Schoenstein F & Jouini N, *J Environ Chem Eng*, 2 (2014) 914.
- 3 Destailats H, Colussi A J, Joseph J M & Hoffmann M R, *J Phys Chem*, 104 (2000) 8930.
- 4 Yang Y, Zhang H, Lee S, Kim D, Hwang W & Wang, Z L, *Nano Lett*, 13 (2013) 803.
- 5 Darwish A A A, Rashad M & AL-Aoh H A, *Dyes Pigm*, 160 (2019) 563.
- 6 Habiba U, Siddique T A, Lee J J L, Joo T C, Ang B C & Afifi A M, *Carbohydr Polym*, 191 (2018) 79.
- 7 Chakraborty A & Acharya H, *Colloids Interf Sci Commun*, 24 (2018) 35.
- 8 Khan M I, Shanableh A, Elboughdiri N, Lashari M H, Manzoor S, Shahida S, Farooq N, Bouazzi Y, Rejeb S, Elleuch Z, Kriaa K & Rehman A U, *ACS Omega*, 7 (2022) 26788.
- 9 Ghani U, Jiang W, Hina K, Idrees A & Iqbal M, *Front Environ Sci*, 10 (2022) 1.
- 10 Qiao C L, Xu Y M, Yin Y, Xu Y X, Xiao Y H & Liu C Q, *Water Sci Technol*, 85 (2022) 2208.
- 11 Danwittayakul S, Jaisai M, Koottatep T & Dutta J, *Ind Eng Chem Res*, 52 (2013) 13629.
- 12 Chamjangali M A, Bagherian G, Javid A, Boroumand S & Farzaneh N, *Spectrochim Acta A: Mol Biomol Spectrosc*, 150 (2015) 230.
- 13 Trandafilovic L V, Jovanovic D J, Zhang X, Ptasinska S & Dramicanin M D, *Appl Catal B: Environ*, 203 (2017) 740.
- 14 Hongzhu Ma, Bo W & Xiaoyan L, *J Hazard Mater*, 149 (2007) 492.
- 15 Ren H P, Tian S P, Zhu M, Zhao Y Z, Li K X, Ma Q, Ding S Y, Gao J & Miao Z, *Appl Clay Sci*, 151 (2018) 29.
- 16 Ren X, Zhang Z, Luo H, Hu B, Dang Z, Yang C & Li L, *Appl Clay Sci*, 97 (2014) 17.
- 17 Wang G, Hua Y, Su X, Komarneni S, Ma S & Wang Y, *Appl Clay Sci*, 124 (2016) 111.
- 18 Khalaf H, Bouras O & Perrichon V, *Microporous Mater*, 8 (1997) 141.
- 19 Kiransan Y, Cheshmehsoltani R D, Hassani A, Karaca S & Khataee A, *J Taiwan Inst Chem Eng*, 45 (2014) 2565.
- 20 Rezala H, Douba H, Boukhatem H & Romero A, *J Chem Soc Pak*, 42 (2020) 550.
- 21 Liu B, Wang X, Yang B & Sun R, *Mater Chem Phys*, 130 (2011) 1220.
- 22 Zhu V, Wang T, Ge F, Chen W & You Z, *J Colloid Interf Sci*, 335 (2009) 77.
- 23 Zhu R, Chen Q, Zhou Q, Xi Y, Zhu J & He H, *Appl Clay Sci*, 123 (2016) 239.
- 24 Rathnayake S I, Xi Y, Frost R L & Ayoko G A, *J Colloid Interf Sci*, 470 (2016) 183.
- 25 Sing K S W, Everett D H, Haul R A W, Moscou L, Pierotti R A, Rouquerol J & Siemieniowska T, *Pure Appl Chem*, 57 (1985) 603.
- 26 Fatimah Is & Huda T, *Appl Clay Sci*, 74 (2013) 115.
- 27 Chen D, Chen J, Luan X, Ji H & Xia Z, *Chem Eng J*, 171 (2011) 1150.
- 28 Gashti M P & Eslami S, *Superlattices Microstruct*, 51 (2012) 135.
- 29 Qin Z, Yuan P, Yang S, Liu D, He H & Zhu J, *Appl Clay Sci*, 99 (2014) 229.
- 30 Mishra A K, Allauddin S, Narayan R, Aminabhavi T M & Raju K V S N, *Ceram Int*, 38 (2012) 929.
- 31 Rathnayake S I, Xi Y, Frost R L & Ayoko G A, *J Colloid Interf Sci*, 459 (2015) 17.
- 32 Ma L, Zhu J, He H, Tao Q, Zhu R, Shen, W & Theng B K G, *Appl Clay Sci*, 101 (2014) 327.
- 33 Liang Y & Li H, *J Mol Liq*, 227 (2017) 139.
- 34 Cabrera-Lafaurie W A, Román F R & Hernández-Maldonado A J, *J Colloid Interf Sci*, 386 (2012) 381.
- 35 Kooli F, *Micropor Mesopor Mat*, 184 (2014) 184.
- 36 Yu W H, Ren Q Q, Tong D S, Zhou C H & Wang H, *Appl Clay Sci*, 97 (2014) 222.
- 37 Xi Y, Frost R L & He H J, *Colloid Interf Sci*, 305 (2007) 150.
- 38 Lagergren S, *Handlingar*, 24 (1898) 1.
- 39 Ho Y S & McKay G, *Process Saf Environ Prot*, 76 (1998) 183.
- 40 Ho Y S & McKay G, *Process Biochem*, 34 (1999) 451.
- 41 Kausar A, Iqbal M, Javed A, Aftab K, Nazli Z H, Bhatti H N & Nouren S, *J Mol Liq*, 256 (2018) 395.
- 42 Goma H, Abd El-Monaem E M, Eltaweil A S, Abdelazeem S & Omer A M, *Scientific Reports*, 12 (2022) 15499.
- 43 Fana X, Zhao B, Maa J, Wang N, Gao W, Gao Y, Zhaoa Yuke & Liub L, *Water Sci Technol*, 86 (2022) 1135.
- 44 Haddadian Z, Shavand M A, Abidin Z Z, Fakhru'l-Razi A & Shah Ismail M H, *Chem Sci Trans*, 2 (2013) 900.
- 45 Abo El Naga A O, Shaban S A & El Kady F Y A, *J Taiwan Inst Chem Eng*, 93 (2018) 363.
- 46 Langmuir I, *J Am Chem Soc*, 38 (1916) 2221.
- 47 Freundlich H M F, *Chemie*, 57 (1906) 385.
- 48 Temkin M J & Pyzhev V, *Acta Phys Chem USSR*, 12 (1940) 217.
- 49 Amin M T, Alazba A A & Shafiq M, *Sustainability*, 7 (2015) 15302.
- 50 Mobarak M, Selim A Q, Mohamed E A & Seliem M K, *J Mol Struct*, 259 (2018) 384.
- 51 Zayed A M, Abdel Wahed M S M, Mohamed E A & Sillanpää M, *Appl Clay Sci*, 166 (2018) 49.
- 52 Kushwaha A K, Gupta N & Chattopadhyaya M C, *J Saudi Chem Soc*, 18 (2014) 200.
- 53 Fan S, Wang Y, Wang Z, Tang J & Li X, *J Environ Chem Eng*, 5 (2017) 601.